King's Research Portal

Document Version
Peer reviewed version

Link to publication record in King's Research Portal

Title: Whole-brain diffusion MRI: a complementary tool for human in vivo cortical parcellation based on a measure of neurite density

Authors: Fernando Calamante[a,b,c], Ben Jeurissen,[d] Robert E. Smith[a], Jacques-Donald Tournier[e,f], Alan Connelly[a,b,c]

Author affiliations:

[a] Florey Institute of Neuroscience and Mental Health, Heidelberg, Victoria, Australia

[b] Florey Department of Neuroscience and Mental Health, University of Melbourne, Melbourne, Victoria, Australia.

[c] Department of Medicine, Austin Health and Northern Health, University of Melbourne, Melbourne, Victoria, Australia.

[d] iMec-Vision Lab, Dept. of Physics, University of Antwerp, Belgium.

[e] Centre for the Developing Brain, King's College London, London, UK.

[f] Department of Biomedical Engineering, King's College London, London, UK.

Corresponding author: Fernando Calamante, Florey Institute of Neuroscience and Mental Health, Melbourne Brain Centre, 245 Burgundy Street, Heidelberg, Victoria 3084, Australia, Phone: (+61 3) 9035 7041, Fax: (+61 3) 9035 7307, Email: fernando.calamante@florey.edu.au

Word count (body of text): 2436

Running title: Diffusion MRI: a complementary tool for myeloarchitecture

Keywords: diffusion MRI, myeloarchitecture, fibre orientation distribution, cortex, parcellation, brain.

ABSTRACT

Purpose: To investigate whether diffusion MRI can be used to parcellate cortical areas based on a contrast related to neurite density, thus providing a complementary tool to myelin-based MRI techniques used for myeloarchitecture.

Methods: Several myelin-sensitive MRI methods (e.g. those based on T_1, T_2, and T_2*) have been proposed to parcellate cortical areas based on their myeloarchitecture. Recent improvements in hardware, acquisition, and analysis methods have opened the possibility of achieving a more robust characterisation of cortical microstructure using diffusion MRI. High-quality diffusion MRI data from the Human Connectome Project was combined with recent advances in fibre orientation modelling. The orientational average of the fibre orientation distribution was used as summary parameter, which was displayed as inflated brain surface views.

Results: Diffusion MRI identifies cortical patterns consistent with those previously seen by MRI methods used for studying myeloarchitecture, which have shown patterns of high myelination in the sensorimotor strip, visual cortex, and auditory areas, and low myelination in frontal and anterior temporal areas.

Conclusion: In vivo human diffusion MRI provides a useful complementary non-invasive approach to myelin-based methods used to study whole-brain cortical parcellation, by exploiting a contrast based on the geometric organisation of the tissue microstructure rather than myelin itself.

KEYWORDS: diffusion MRI, myeloarchitecture, fibre orientation distribution, cortex, parcellation, brain.

INTRODUCTION

The arrangement and density of myelinated fibres throughout the cortex is greatly heterogeneous (1). The spatial organization of these myelinated fibres in the cortex makes it possible to parcellate areas based on their myeloarchitecture, due to differences in the properties (e.g. their thickness and compactness) of the fibre layers and radial fibres (1). Myeloarchitecture and cytoarchitecture have long been used for cortical parcellation; while the former is based on the arrangement of myelinated fibres, the latter is based on the size, shape and arrangement of neuronal cell bodies.

Invasive techniques for myeloarchitecture have been around for over a century (e.g. staining myelinated nerve fibres using the Weigert stain or its variants) (1–5). More recently, the use of non-invasive MRI methods to map cortical myeloarchitecture has received increasing interest. For example, a number of methods based on T_1-, T_2- and T_2*-weighted images (or on their quantitative parameters T_1, T_2 and T_2*), as well as on magnetisation transfer ratio and quantitative susceptibility mapping have been shown to produce detailed maps of human cortical areas in a completely non-invasive way (6–17). Many of these studies have consistently shown image contrast (e.g. low vs. high T_1 values) between well-defined areas, on the one hand corresponding to areas previously shown to have high myelination (e.g. with low T_1 values, such as in the sensorimotor strip in the central sulcus, visual cortex, and auditory areas in the Sylvian fissure), and on the other corresponding to areas previously shown to have low myelination (e.g. with high T_1 values, such as in frontal areas).

Recent improvements in MRI hardware, acquisition methods, and higher-order models for the diffusion MRI signal have opened the possibility of achieving a more robust characterisation of the microstructure properties of cortical grey matter (GM) using diffusion MRI. Diffusion MRI may therefore provide an alternative useful contrast to study GM, despite having previously focused primarily on white matter (WM). Most diffusion MRI studies of GM so far have been mainly aimed at providing detailed intra-cortical information (18–24), and most often this has been achieved based on high-resolution *ex vivo* diffusion MRI data. Some other studies (25,26) have also shown promising *in vivo* results for exploiting the diffusion MRI contrast to delineate cortical features that were spatially consistent with previous myeloarchitecture studies. For example, McNab et al (25) scanned at high resolution (1 mm isotropic) a coronal slab of the

3

human brain that covered the primary motor cortex (M1) and primary somatosensory cortex (S1), and used a surface-based analysis to investigate the principal diffusion orientation (based on the diffusion tensor model), the fractional anisotropy and the mean diffusivity; in particular, they found that the principal diffusion orientation was able to differentiate specific regions, including M1 (with primarily radial orientation), S1 (primarily tangential), as well as Heschl's gyrus and second somatosensory cortex (S2) (primarily tangential). Similarly, Nagy et al (26) used several features extracted from diffusion signal profiles (obtained from whole-brain at 2.3 mm resolution) to discriminate a number of cortical regions in the human brain. However, further investigations in whole-brain *in vivo* human data are still required to assess whether diffusion MRI can be used to map human cortical areas based on a contrast related to cortical microstructure, and thus provide a complementary non-invasive tool to the myelin-based MRI techniques increasingly being used for whole-brain *in vivo* cortical parcellation. We investigate this here by exploiting high-quality diffusion MRI data (27,28) and recent advances in diffusion fibre orientation modelling (29).

METHODS

Data acquisition

Data from 8 healthy subjects were acquired on a Siemens 3T Connectome Skyra system with a 32-channel head coil as part of the Human Connectome Project (27,28); these data were downloaded from the ConnectomeDB (http://db.humanconnectome.org). The relevant diffusion MRI parameters include: 18 b=0 images and b=1000, 2000 and 3000 s/mm^2 (90 diffusion directions each); TR/TE=5520/89.5 ms (which were matched across shells); 1.25mm isotropic resolution. In addition, all images were acquired with reversed phase-encoding for susceptibility distortion correction. Structural scans were also acquired for every subject, using high-resolution T_1-weighted imaging (0.7 mm isotropic). Please refer to references (27,28) for further details regarding acquisition and pre-processing steps – Note: any further processing step besides those standard for the HCP data are described in the next section. The signal-to-noise ratios were 19.1, 7.8, 4.7, and 3.4 for the b=0, 1000, 2000 and 3000 s/mm^2, respectively, with signal-to-noise ratio for a given b value defined as the ratio of the mean signal for the b images to the standard deviation of the b=0 signal.

Data Analysis

Diffusion MRI analysis was carried out using *MRtrix* (http://www.mrtrix.org). Fibre orientation distributions (FODs) were calculated using multi-shell multi-tissue (MSMT) constrained spherical deconvolution (CSD) (29). In brief, MSMT-CSD is an extension of single-shell CSD (30) to multi-shell diffusion MRI data, and it involves a multi-compartment model that can be used to resolve different components (in our case, WM-like, GM-like, and cerebrospinal fluid like components) based on their distinct b-value dependences. MSMT-CSD produces an estimate of each of these components, with the WM-like compartment also characterised as a full FOD (29). In particular, and of relevance for the current study, the measurement of the WM-like component within cortical GM can be non-zero. Prior to MSMT-CSD, the diffusion-weighted images were corrected for bias-fields as these could introduce a spatial dependency in the scaling of the tissue responses. For each subject, a single multiplicative bias field was estimated using the $b = 0$ s/mm^2 images and the N4ITK approach (31). The estimated bias field was then applied to correct the intensity of all diffusion-weighted volumes.

To study cortical patterns, the l=0 term of the FOD spherical harmonic expansion of the WM-like component (i.e. the orientational average of the FOD, which corresponds to the density of the WM-like component) was computed in each cortical voxel. For consistency with the terminology previously used in the apparent fibre density (AFD) method (32), this l=0 term is referred to as AFD_{total} (33), since it corresponds to the AFD summed over all orientations.

After rigid realignment of the T$_1$-weighted anatomical data to the diffusion MRI data, the cortical distribution of AFD_{total} values are displayed as inflated brain surface views using FreeSurfer (http://surfer.nmr.mgh.harvard.edu). For the results shown here, AFD_{total} was sampled along the normal between the WM/GM interface and the pial surface for a total of 11 equally spaced samples; these values were then averaged, and projected back onto the mid-cortical surface. Note: To verify that partial volume effect with adjacent WM was not the source of the observed effect, the analysis was repeated excluding the contribution from the 3 cortical subdivisions closer to the WM/GM interface – see Supporting Fig. S1.

For comparison, and to assess the effect of using advanced diffusion fibre orientation modelling, the same analysis was repeated for the FODs estimated from single-shell data (corresponding to the b=3000 s/mm^2 shell), using the single-tissue CSD method, as implemented in reference (29).

RESULTS

Consistent with previous findings (29), Fig. 1 confirms that the recently proposed MSMT-CSD approach provides a much more robust estimate of the fibre architecture in the cortex than that obtained using single-shell single-tissue CSD (cf. Figs. 1a and 1b): the predominant radial fibre orientation is more clearly identified with MSMT-CSD than with CSD. Interestingly, the smaller FODs observed in certain cortical structures are not artefactual, but their spatial distribution does correspond with the known myeloarchitecture patterns observed with myelin-based methods. For example, close inspection of the FODs in Fig. 1a shows a change in the cortical microstructure (e.g. as given by a change in the overall size of the FODs) that is anatomically consistent with the known transition between the high myelin Brodmann area 4 and low myelin Brodmann area 3a (arrow), as seen in previous T_1 and myelin histology studies (see Figs. 1d and 1e) (10). It should be emphasised, however, that diffusion MRI is primarily sensitive to the presence and organisation of 'WM-like' fibres in the cortex; it is not clear to what extent the myelin content itself contributes to the effect observed in the diffusion MRI data (34) – see Discussion section for further details.

When displayed on an axial orientation, the MSMT-CSD approach also reproduces the expected different dominant fibre orientation in the neighbourhood of the central sulcus (Fig. 2), with M1 showing a primarily radial dominant orientation and S1 mostly a tangential orientation (e.g. cf. Fig. 1 of MacNab et al (25)).

The overall microstructure pattern based on MSMT-CSD data is shown in Figs. 3a and 3b, where the group average results of AFD_{total} from MSMT-CSD are shown (see Figs. 4a and 4b for the corresponding results from an illustrative individual): the location of areas of high AFD_{total} show a striking similarity to well-characterised areas of high myelin (e.g. cf. Fig. 3 of Glasser et al (12)), including sensorimotor strip, auditory areas, visual cortex (V1, V2) and other areas involved in visual processing (e.g. medial temporal complex, MT+, and frontal eye fields, FEF). It also shows low AFD_{total} areas in well-recognised areas of low myelin (e.g. frontal areas, anterior temporal, etc.). Note: the AFD_{total} patterns were very similar when the contribution from the 3 cortical subdivisions closer to the GM/WM interface were excluded (see Supporting Fig. S1; and the Spearman's coefficient showed high spatial correlation between the two maps, with $\rho=0.95$), suggesting partial volume effect with WM is not responsible for the observed effect.

Interestingly, Fig. 1c shows that areas with reduced AFD_{total} are not necessarily devoid of coherent fibre architecture, but that they are mostly reduced in their overall magnitude (cf. Figs. 1a and 1c).

As a measure of the inter-group variability on the AFD_{total} patterns, Supporting Fig. S2 shows the group standard deviation maps. While the variance is, in general, larger in cortical regions with larger AFD_{total} values, the patterns are not equivalent. For example, frontal areas have very low AFD_{total} but some have relatively large variance. Similarly, despite comparable AFD_{total} values in primary motor and sensory areas (e.g. 'SM' label in Fig. 3b), the variance was smaller in primary motor cortex; this finding was consistent with the variance patterns observed with myelin-based methods (35).

In contrast to MSMT-CSD, the spatial patterns observed with AFD_{total} from single-shell single-tissue CSD do not reflect the myeloarchitecture patterns based on methods sensitive to myelin distribution (see Figs. 3c and 3d); the difference in cortical patterns between MSMT and single-shell single-tissue CSD is presumably due to partial volume with the isotropic components of GM and cerebrospinal fluid (36).

As can be appreciated from the cortical thickness map (Fig. 5), and consistent with previous studies (8), the microstructure patterns observed with MSMT-CSD are not simply due to thickness-related effects (i.e. the patterns are not equivalent). Spearman's coefficient showed low spatial correlation between the two maps ($\rho = -0.11$).

DISCUSSION

We have shown that whole-brain *in vivo* human diffusion MRI can identify cortical patterns consistent with those previously shown with myelin-based methods used for studying myeloarchitecture (6–17). This was made possible by combining high-quality MRI data with advanced diffusion MRI models. Diffusion MRI therefore provides a promising and complementary non-invasive approach to myelin-based methods in the study of whole-brain cortical parcellation, by exploiting a contrast based on tissue microstructure organisation. Our results also complement previous work on cortical measurements in diffusion MRI (18–26).

It should be noted that, as was the case for the more general AFD formalism (32), AFD_{total} can be used quantitatively, therefore providing a useful complementary surrogate marker to study cortical patterns in the healthy and diseased brain.

Given that the CSD formalism (both for the single and multi-shell variants) involves no normalisation to the $b=0$ image (cf. for example to the apparent diffusion coefficient formalism), AFD_{total} could still have contribution from T_1 and T_2. However, it should be emphasized that the observed AFD_{total} cortical patterns were not due to residual T_1 and T_2-weighting in the diffusion MRI data, given that they were not present in the single-shell single-tissue CSD results, which were acquired using the same TE/TR values. They must therefore be related to the diffusion contrast mechanism.

The cortical patterns observed also cannot be explained simply by a cortical thickness 'partial volume' effect, i.e. mainly reflecting contamination from partial volume with the anisotropic component in the white matter fraction of the voxel (and, therefore, not related to the cortical tissue). As shown in Fig. 5, the cortical thickness patterns are substantially different to those patterns found in AFD_{total}. These findings are consistent with those from previous studies: for example, using a T_2*-based myeloarchitecture method, Cohen-Adad et al (8) showed that, while there can be some regions of low/high T_2* that correspond to thick/thin cortex, quantitatively the maps had low spatial correlation, from which they concluded that the myeloarchitecture patterns could not be the result of cortical thickness effects alone.

The observed cortical AFD_{total} patterns have, in general, a bilateral appearance. There are however some exceptions: these include the auditory areas, where larger AFD_{total} values were observed on the left hemisphere (Fig. 3). This left-right asymmetry is consistent with the results found by others, such as the lower T_2* values in Brodmann area 42 on the left hemisphere by Cohen-Adad et al (8), and higher R_1 values reported by (37), likely related to the greater myelination in left auditory cortex. We also observed a left-right asymmetry in the primary somatosensory cortex, where AFD_{total} in the left hemisphere had a smaller extent towards the ventral aspect. This finding is somewhat surprising, as it has not been reported using most myeloarchitecture surrogate markers (12); however, there have been reports of inter-hemispheric differences in Brodmann areas 2–3 (consistent with our observations in AFD_{total} patterns) based

on T_2* myeloarchitectonics (8). Further studies are therefore required to understand the exact source of this left-right asymmetry within S1.

As highlighted in the Results section, it should be emphasised that, while AFD_{total} from MSMT-CSD provided useful complementary information to myeloarchitecture, this does not imply that the observed diffusion contrast is primarily due to the presence of myelin (34). The presence of myelin does have an influence on the measured diffusion signal and its anisotropy, but it has been shown that it is not the key contribution, which is instead the density of intact membranes (34). In fact, given that anisotropy can be measured even in healthy non-myelinated fibres, it has been stressed that diffusion anisotropy should not be considered myelin-specific (38). The AFD_{total} contrast reflects instead the density of WM-like fibres in the cortex, and is more likely related to the changes in microstructural properties often seen in those cortical areas (1): variations in the proportion and density of radial/tangential fibres in the cortex defines the various myeloarchitectonic areas.

By definition, AFD_{total} corresponds to the AFD summed over all orientations. Based on numerical simulations, Raffelt et al (32) showed that, under certain experimental conditions (e.g. high b-value and long diffusion-weighting gradient pulses), the signal in the diffusion-weighted imaging originates primarily from the restricted compartment, and that the orientational averaged AFD can be considered proportional to neurite density (see reference (32) for further discussion regarding the interpretation of AFD and the experimental conditions under which this is valid). AFD_{total} would be expected to correlate strongly with myelin if the axons/neurites contributing to the AFD_{total} signal were myelinated uniformly; however, there is scope for the non-myelinated axons/neurites to contribute to the AFD_{total} without a corresponding contribution to the myelin signal. More generally, while we expect to see this correlation, it would be very speculative to therefore interpret AFD_{total} as a marker of myelin. Other diffusion MRI parameters might be also suitable to generate similar cortical patterns to those observed here using AFD_{total}, such as those based on complex models of microstructure like neurite orientation dispersion and density imaging (NODDI) (39) and others. Further work is needed to determine the relative performance of the various possible diffusion MRI parameters, their noise sensitivity, etc. It is again important to emphasise, however, that all these diffusion MRI measures are not myelin-based measures and, therefore, their cortical patterns are not expected to match one-to-one with the patterns observed with more myelin-sensitive techniques commonly used for myeloarchitecture, such as

9

with T_1-weighted/T_2-weighted imaging (12). It should be therefore stressed that AFD_{total} (and other related diffusion MRI measures) cannot be considered tools for myeloarchitecture, but rather that they can complement these other myelin-based methods. Further studies are required to determine how the patterns observed with these diffusion-based methods relate to those seen with myelin-based methods, but this is beyond the scope of this Technical Note, whose main purpose is to introduce AFD_{total} as a tool for cortical parcellation.

Our observations based on AFD_{total} may also have implications for those interested in continuing the streamline tracking process into cortical structures (instead of typically stopping when the streamline exit WM tissue, e.g. based on a FOD or fractional anisotropy threshold). For example, apart from the known issues for tractography algorithms related to the presence of high curvature for streamlines when reaching some cortical areas and the associated gyral bias (40), as well as the effect from superficial white matter fibres (41), the observed cortical AFD_{total} patterns may also influence streamline terminations (e.g. areas with low AFD_{total} may fall below an FOD threshold used for terminating tracking (29,42), and thus the degree of streamline tracking into cortical structures will be biased by the AFD_{total} patterns).

Finally, it should be noted that the results presented here were achieved using high-quality data from the Human Connectome Project, acquired on a customised 3T system using a relatively long acquisition protocol; these data are therefore far superior to those typically achievable with more conventional 3T scanners and diffusion MRI acquisition protocols. It remains to be investigated whether AFD_{total} also provides a viable option for investigations into cortical microstructure using more standard diffusion MRI data and, if so, what the optimal acquisition protocol should be.

CONCLUSIONS

This study demonstrates that in vivo human diffusion MRI may provide a useful complementary non-invasive approach to myelin-based methods used to study whole-brain cortical parcellation, by exploiting a contrast based on a diffusion MRI-derived measure of neurite density, rather than myelin itself. Given the difference in the mechanism underlying the contrast, it is possible that the combination of this approach with *in vivo* myelin mapping methods (such as those based on T_1- and T_2*-weighted data (12,15)) will allow more detailed investigations into the organisation

of the human cortex, its function, and associated pathologies, particularly in regions where these patterns do not match.

ACKNOWLEDGEMENTS

REFERENCES

1. Nieuwenhuys R. The myeloarchitectonic studies on the human cerebral cortex of the Vogt-Vogt school, and their significance for the interpretation of functional neuroimaging data. Brain Struct. Funct. 2013;218:303–352. doi: 10.1007/s00429-012-0460-z.

2. Vogt O. Zur anatomischen Gliederung des Cortex cerebri. J Psychol Neurol 1903;2:160–180.

3. Vogt C, Vogt O. Allgemeinere Ergebnisse unserer Hirnforschung. J. Psychol. Neurol. 1919;25:279–461.

4. Hopf A. Photometric studies on the myeloarchitecture of the human temporal lobe. J. Hirnforsch. 1968;10:285–297.

5. Nieuwenhuys R, Broere CAJ. A map of the human neocortex showing the estimated overall myelin content of the individual architectonic areas based on the studies of Adolf Hopf. Brain Struct. Funct. 2017;222:465–480. doi: 10.1007/s00429-016-1228-7.

6. Barazany D, Assaf Y. Visualization of cortical lamination patterns with magnetic resonance imaging. Cereb. Cortex N. Y. N 1991 2012;22:2016–2023. doi: 10.1093/cercor/bhr277.

7. Cohen-Adad J. What can we learn from T2* maps of the cortex? NeuroImage 2014;93 Pt 2:189–200. doi: 10.1016/j.neuroimage.2013.01.023.

8. Cohen-Adad J, Polimeni JR, Helmer KG, Benner T, McNab JA, Wald LL, Rosen BR, Mainero C. T_2* mapping and B_0 orientation-dependence at 7 T reveal cyto- and

myeloarchitecture organization of the human cortex. NeuroImage 2012;60:1006–1014. doi: 10.1016/j.neuroimage.2012.01.053.

9. Dinse J, Härtwich N, Waehnert MD, Tardif CL, Schäfer A, Geyer S, Preim B, Turner R, Bazin P-L. A cytoarchitecture-driven myelin model reveals area-specific signatures in human primary and secondary areas using ultra-high resolution in-vivo brain MRI. NeuroImage 2015;114:71–87. doi: 10.1016/j.neuroimage.2015.04.023.

10. Geyer S, Weiss M, Reimann K, Lohmann G, Turner R. Microstructural Parcellation of the Human Cerebral Cortex - From Brodmann's Post-Mortem Map to in vivo Mapping with High-Field Magnetic Resonance Imaging. Front. Hum. Neurosci. 2011;5:19. doi: 10.3389/fnhum.2011.00019.

11. Glasser MF, Goyal MS, Preuss TM, Raichle ME, Van Essen DC. Trends and properties of human cerebral cortex: correlations with cortical myelin content. NeuroImage 2014;93 Pt 2:165–175. doi: 10.1016/j.neuroimage.2013.03.060.

12. Glasser MF, Van Essen DC. Mapping human cortical areas in vivo based on myelin content as revealed by T1- and T2-weighted MRI. J. Neurosci. Off. J. Soc. Neurosci. 2011;31:11597–11616. doi: 10.1523/JNEUROSCI.2180-11.2011.

13. Govindarajan ST, Cohen-Adad J, Sormani MP, Fan AP, Louapre C, Mainero C. Reproducibility of T2 * mapping in the human cerebral cortex in vivo at 7 tesla MRI. J. Magn. Reson. Imaging JMRI 2015;42:290–296. doi: 10.1002/jmri.24789.

14. Lutti A, Dick F, Sereno MI, Weiskopf N. Using high-resolution quantitative mapping of R1 as an index of cortical myelination. NeuroImage 2014;93 Pt 2:176–188. doi: 10.1016/j.neuroimage.2013.06.005.

15. Mangeat G, Govindarajan ST, Mainero C, Cohen-Adad J. Multivariate combination of magnetization transfer, T2* and B0 orientation to study the myelo-architecture of the in vivo human cortex. NeuroImage 2015;119:89–102. doi: 10.1016/j.neuroimage.2015.06.033.

16. Marques JP, Khabipova D, Gruetter R. Studying cyto and myeloarchitecture of the human cortex at ultra-high field with quantitative imaging: R1, R2(*) and magnetic susceptibility. NeuroImage 2017;147:152–163. doi: 10.1016/j.neuroimage.2016.12.009.

17. Van Essen DC, Glasser MF. In vivo architectonics: a cortico-centric perspective. NeuroImage 2014;93 Pt 2:157–164. doi: 10.1016/j.neuroimage.2013.04.095.

18. Aggarwal M, Nauen DW, Troncoso JC, Mori S. Probing region-specific microstructure of human cortical areas using high angular and spatial resolution diffusion MRI. NeuroImage 2015;105:198–207. doi: 10.1016/j.neuroimage.2014.10.053.

19. Bastiani M, Oros-Peusquens A-M, Seehaus A, et al. Automatic Segmentation of Human Cortical Layer-Complexes and Architectural Areas Using Ex vivo Diffusion MRI and Its Validation. Front. Neurosci. 2016;10:487. doi: 10.3389/fnins.2016.00487.

20. Budde MD, Annese J. Quantification of anisotropy and fiber orientation in human brain histological sections. Front. Integr. Neurosci. 2013;7:3. doi: 10.3389/fnint.2013.00003.

21. Kleinnijenhuis M, van Mourik T, Norris DG, Ruiter DJ, van Cappellen van Walsum A-M, Barth M. Diffusion tensor characteristics of gyrencephaly using high resolution diffusion MRI in vivo at 7T. NeuroImage 2015;109:378–387. doi: 10.1016/j.neuroimage.2015.01.001.

22. Kleinnijenhuis M, Zerbi V, Küsters B, Slump CH, Barth M, van Cappellen van Walsum A-M. Layer-specific diffusion weighted imaging in human primary visual cortex in vitro. Cortex J. Devoted Study Nerv. Syst. Behav. 2013;49:2569–2582. doi: 10.1016/j.cortex.2012.11.015.

23. Leuze CWU, Anwander A, Bazin P-L, Dhital B, Stüber C, Reimann K, Geyer S, Turner R. Layer-specific intracortical connectivity revealed with diffusion MRI. Cereb. Cortex N. Y. N 1991 2014;24:328–339. doi: 10.1093/cercor/bhs311.

24. Truong T-K, Guidon A, Song AW. Cortical depth dependence of the diffusion anisotropy in the human cortical gray matter in vivo. PloS One 2014;9:e91424. doi: 10.1371/journal.pone.0091424.

25. McNab JA, Edlow BL, Witzel T, et al. The Human Connectome Project and beyond: initial applications of 300 mT/m gradients. NeuroImage 2013;80:234–245. doi: 10.1016/j.neuroimage.2013.05.074.

26. Nagy Z, Alexander DC, Thomas DL, Weiskopf N, Sereno MI. Using high angular resolution diffusion imaging data to discriminate cortical regions. PloS One 2013;8:e63842. doi: 10.1371/journal.pone.0063842.

27. Sotiropoulos SN, Jbabdi S, Xu J, et al. Advances in diffusion MRI acquisition and processing in the Human Connectome Project. NeuroImage 2013;80:125–143. doi: 10.1016/j.neuroimage.2013.05.057.

28. Van Essen DC, Smith SM, Barch DM, Behrens TEJ, Yacoub E, Ugurbil K, WU-Minn HCP Consortium. The WU-Minn Human Connectome Project: an overview. NeuroImage 2013;80:62–79. doi: 10.1016/j.neuroimage.2013.05.041.

29. Jeurissen B, Tournier J-D, Dhollander T, Connelly A, Sijbers J. Multi-tissue constrained spherical deconvolution for improved analysis of multi-shell diffusion MRI data. NeuroImage 2014;103:411–426. doi: 10.1016/j.neuroimage.2014.07.061.

30. Tournier J-D, Calamante F, Connelly A. Robust determination of the fibre orientation distribution in diffusion MRI: non-negativity constrained super-resolved spherical deconvolution. NeuroImage 2007;35:1459–1472.

31. Tustison NJ, Avants BB, Cook PA, Zheng Y, Egan A, Yushkevich PA, Gee JC. N4ITK: improved N3 bias correction. IEEE Trans. Med. Imaging 2010;29:1310–1320. doi: 10.1109/TMI.2010.2046908.

32. Raffelt D, Tournier J-D, Rose S, Ridgway GR, Henderson R, Crozier S, Salvado O, Connelly A. Apparent Fibre Density: a novel measure for the analysis of diffusion-weighted magnetic resonance images. NeuroImage 2012;59:3976–3994. doi: 10.1016/j.neuroimage.2011.10.045.

33. Calamante F, Smith RE, Tournier J-D, Raffelt D, Connelly A. Quantification of voxel-wise total fibre density: Investigating the problems associated with track-count mapping. NeuroImage 2015;117:284–293. doi: 10.1016/j.neuroimage.2015.05.070.

34. Beaulieu C. The basis of anisotropic water diffusion in the nervous system - a technical review. NMR Biomed. 2002;15:435–455. doi: 10.1002/nbm.782.

35. Robinson EC, Jbabdi S, Glasser MF, Andersson J, Burgess GC, Harms MP, Smith SM, Van Essen DC, Jenkinson M. MSM: a new flexible framework for Multimodal Surface Matching. NeuroImage 2014;100:414–426. doi: 10.1016/j.neuroimage.2014.05.069.

36. Roine T, Jeurissen B, Perrone D, Aelterman J, Leemans A, Philips W, Sijbers J. Isotropic non-white matter partial volume effects in constrained spherical deconvolution. Front. Neuroinformatics 2014;8:28. doi: 10.3389/fninf.2014.00028.

37. Sigalovsky IS, Fischl B, Melcher JR. Mapping an intrinsic MR property of gray matter in auditory cortex of living humans: a possible marker for primary cortex and hemispheric differences. NeuroImage 2006;32:1524–1537. doi: 10.1016/j.neuroimage.2006.05.023.

38. Beaulieu C. What Makes Diffusion Anisotropic in the Nervous System? In: Jones DK, editor. Diffusion MRI. Oxford, UK: Oxford University Press; 2010. pp. 92–109.

39. Zhang H, Schneider T, Wheeler-Kingshott CA, Alexander DC. NODDI: practical in vivo neurite orientation dispersion and density imaging of the human brain. NeuroImage 2012;61:1000–1016. doi: 10.1016/j.neuroimage.2012.03.072.

40. Van Essen DC, Jbabdi S, Sotiropoulos SN, Chen C, Dikranian K, Coalson T, Harwell J, Behrens TEJ, Glasser MF. Chapter 16 - Mapping Connections in Humans and Non-Human Primates: Aspirations and Challenges for Diffusion Imaging. In: Diffusion MRI (Second Edition). San Diego: Academic Press; 2014. pp. 337–358.

41. Reveley C, Seth AK, Pierpaoli C, Silva AC, Yu D, Saunders RC, Leopold DA, Ye FQ. Superficial white matter fiber systems impede detection of long-range cortical connections in diffusion MR tractography. Proc. Natl. Acad. Sci. U. S. A. 2015;112:E2820-2828. doi: 10.1073/pnas.1418198112.

42. Tournier J-D, Calamante F, Connelly A. MRtrix: Diffusion tractography in crossing fiber regions. Int. J. Imaging Syst. Technol. 2012;22:53–66.
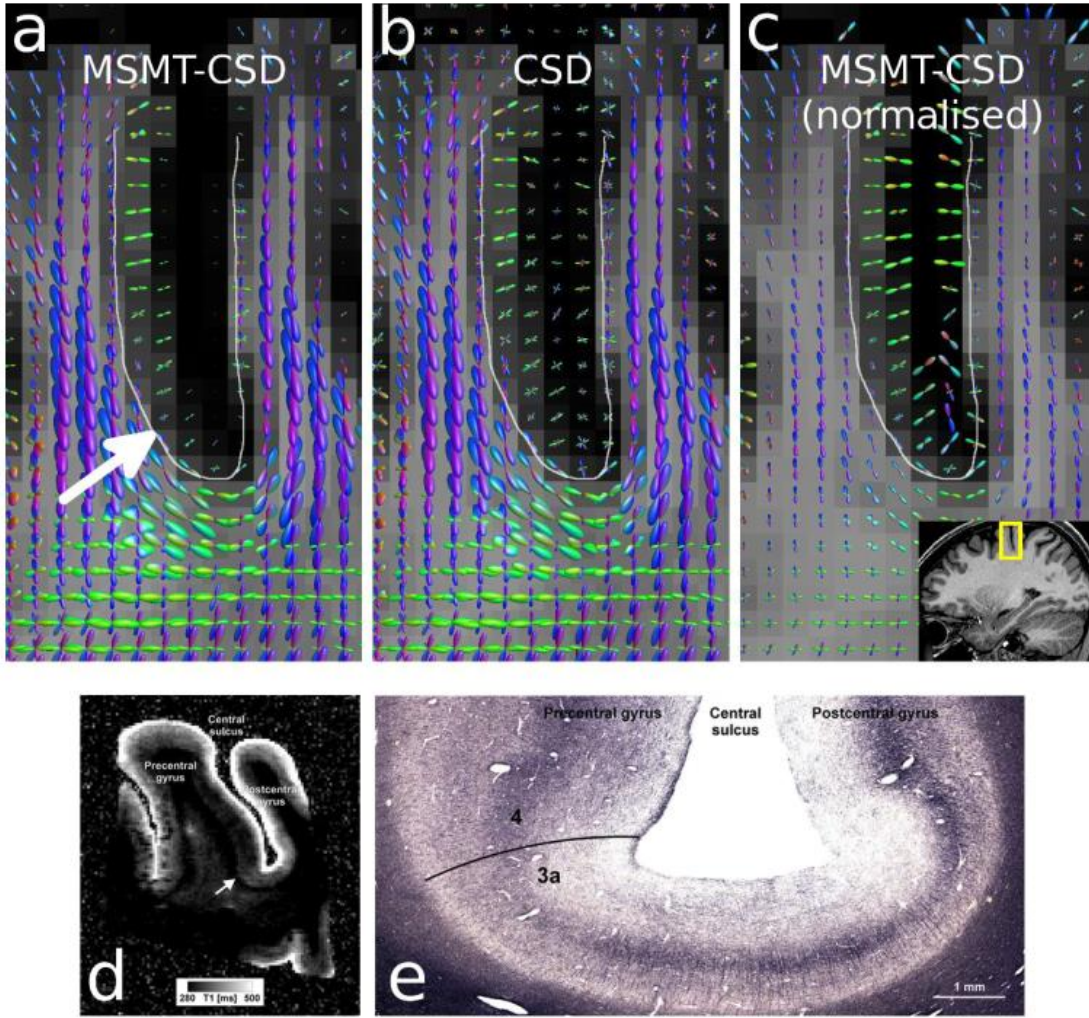
Figure 1: Fibre orientation distributions (FODs) in the border between primary motor (Brodmann area 4) and somatosensory (Brodmann area 3a) cortex in a single subject (see inset in (c) for location); calculated using MSMT-CSD (a) or standard (single-shell single tissue) CSD (b). (c) Same FODs as in (a), but normalised to unit AFD_{total}. The solid line curve in included to provide an indication of the location of the WM/GM boundary. Arrow in (a) indicates the transition between Brodmann area 4 and Brodmann area 3a. (d) Ex vivo quantitative T_1 map of a tissue block of the border between areas 4 and 3a from a post-mortem human brain (Note: different brain to that shown in (a)–(c)); arrow indicates a sharp change in T_1 contrast that is consistent with the change in myelin, as seen by staining for myelin basic protein (e). Panels (d) and (e) reproduced with permission from (10), © 2011 Geyer, Weiss, Reimann, Lohmann and Turner.
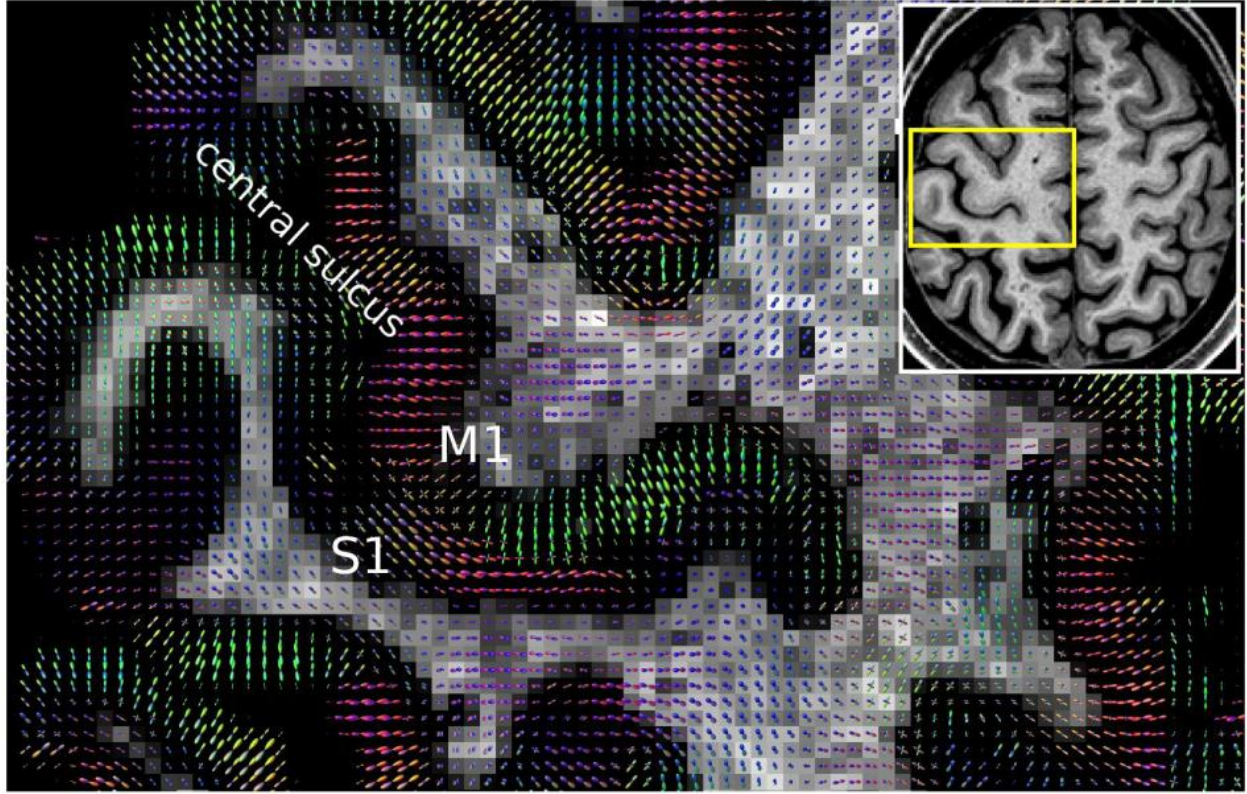
Figure 2: Fibre orientation distributions (FODs) overlaid on an anatomical image, in the neighbourhood of the central sulcus. The insert image shows the anatomical axial slice, as well as the zoomed region where the FODs are overlaid. M1 (on the anterior side of the central sulcus in the image) displays a mostly radial orientation; S1 (on the posterior side) displays primarily tangential orientation. The FODs have been normalised to unit AFD_{total} for ease of visualisation of the orientations.
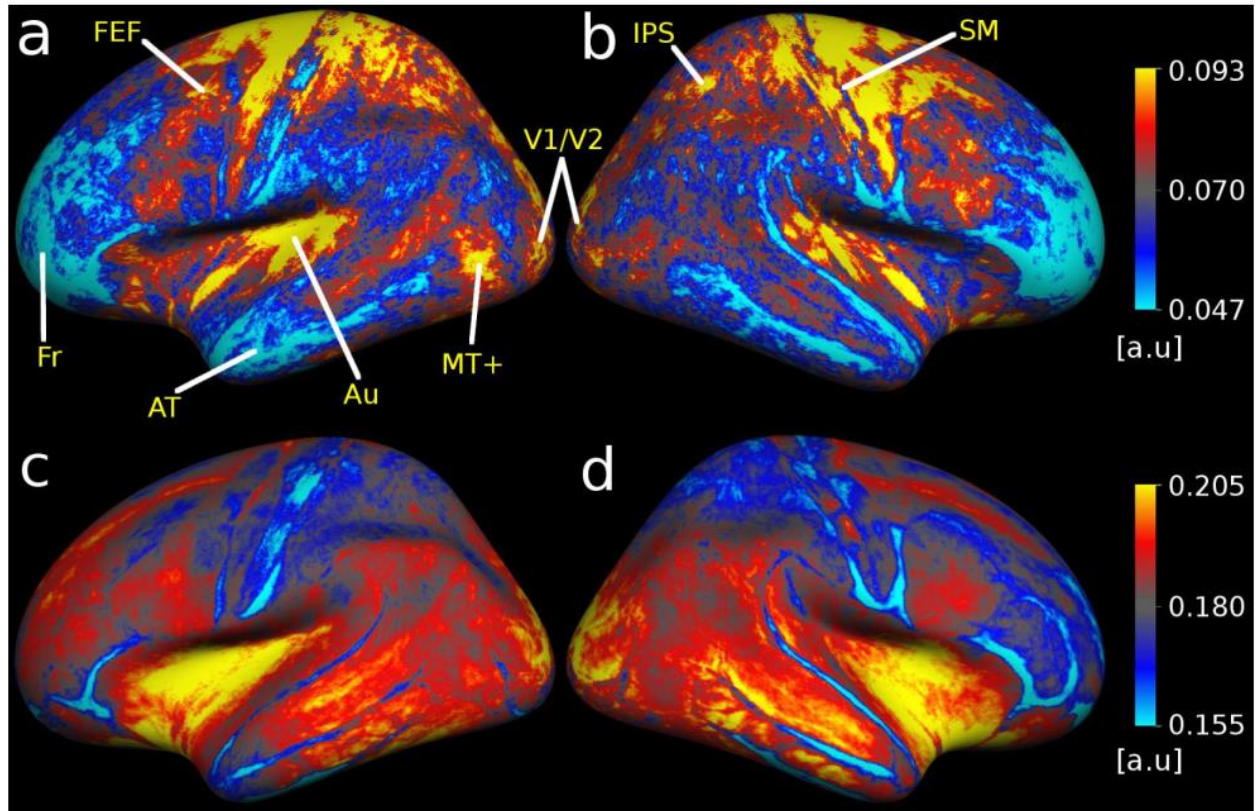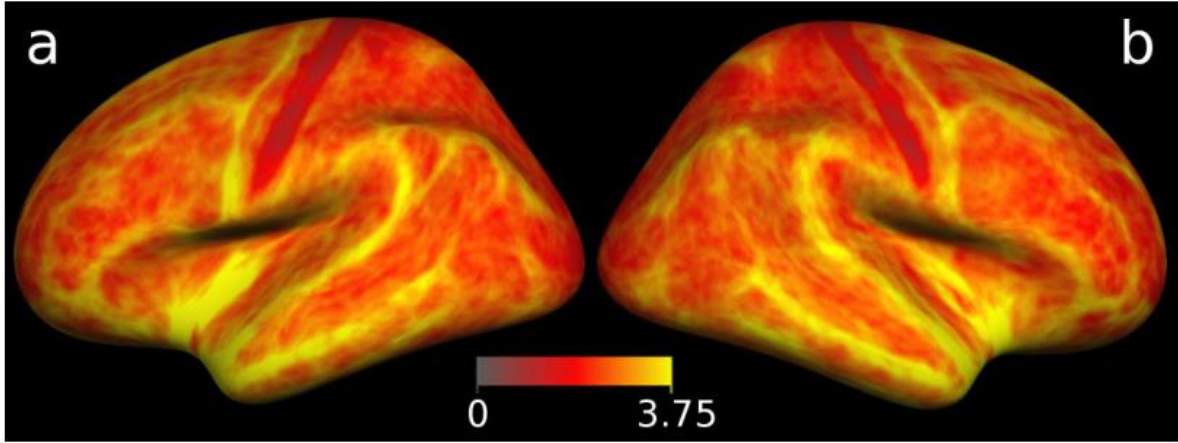
Figure 3: Group average (N=8) *AFD*_{total} maps displayed on an inflated surface, from MSMT-CSD (a: left, b: right hemispheres), and from single-shell single-tissue CSD (c: left, d: right). The *AFD*_{total} cortical patterns reconstructed based on data from MSMT-CSD show a striking similarity with well-known patterns of myeloarchitecture. Au: auditory; AT: anterior temporal; FEF: frontal eye fields; Fr: Frontal; IPS: intra-parietal sulcus; MT+: middle temporal complex; SM: sensorimotor; V1: primary visual cortex; and V2: visual area two. A.u.: arbitrary units.
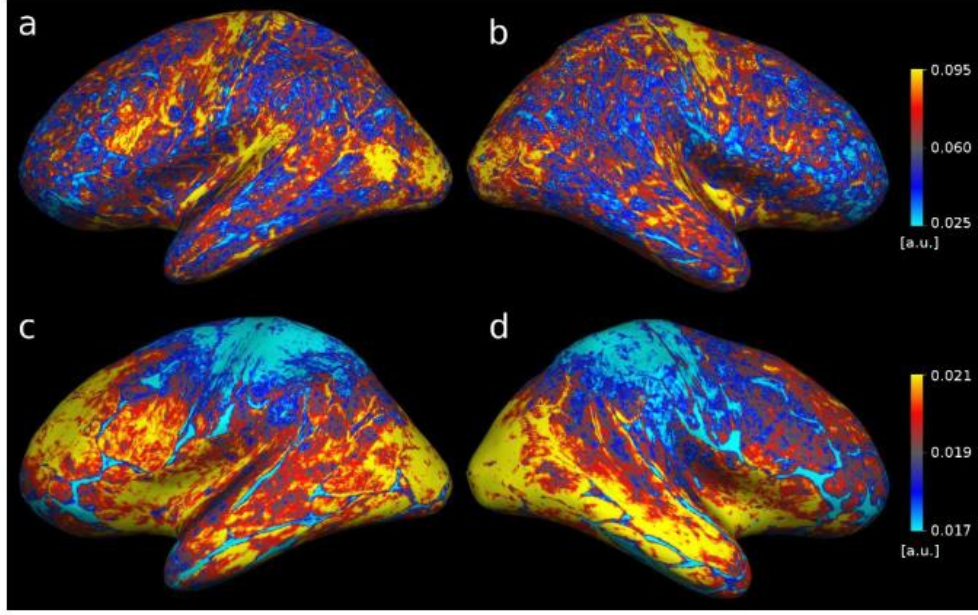
Figure 4: *AFD_{total}* AFD_{total} map from an illustrative individual, displayed on an inflated surface. The results from MSMT-CSD are shown at the top (a: left, b: right hemispheres); the results from single-shell single-tissue CSD at the bottom (c: left, d: right). Similar patterns to those observed in the population average can be seen with MSMT-CSD (cf. Fig. 3, top row), albeit noisier, as expected. A.u.: arbitrary units.

Figure 5: Population average cortical thickness map (in mm), displayed on an inflated surface (a: left, b: right hemispheres). There is no one-to-one match between the AFD_{total} patterns and the thickness patterns.
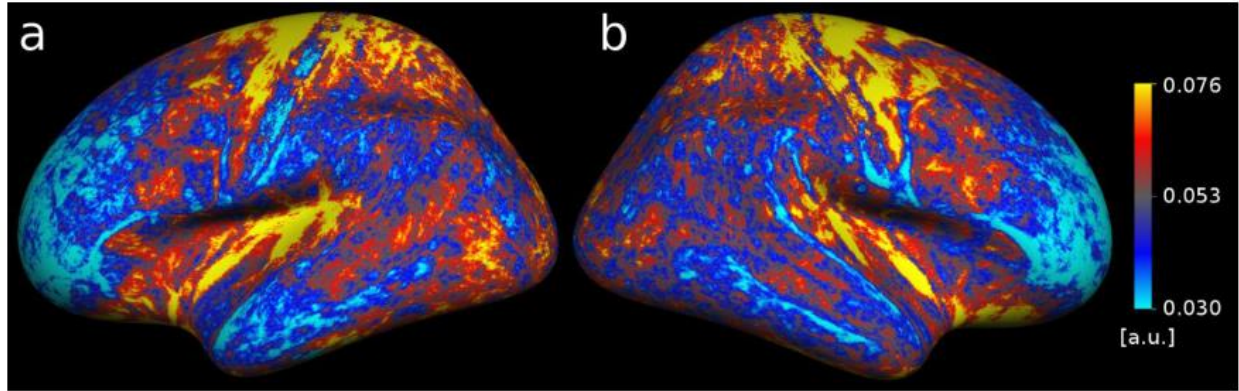
Supporting Figure S1: Group average (N=8) AFD_{total} maps displayed on an inflated surface, from MSMT-CSD (a: left, b: right hemispheres). The AFD_{total} here was computed by excluding the contribution from the 3 cortical subdivisions closer to the GM/WM interface. The AFD_{total} patterns were very similar to those shown in the top row of Fig. 3 (where the contributions from all cortical subdivisions were included in the AFD_{total} calculation), suggesting partial volume effect is not responsible for the observed effect. A.u.: arbitrary units.
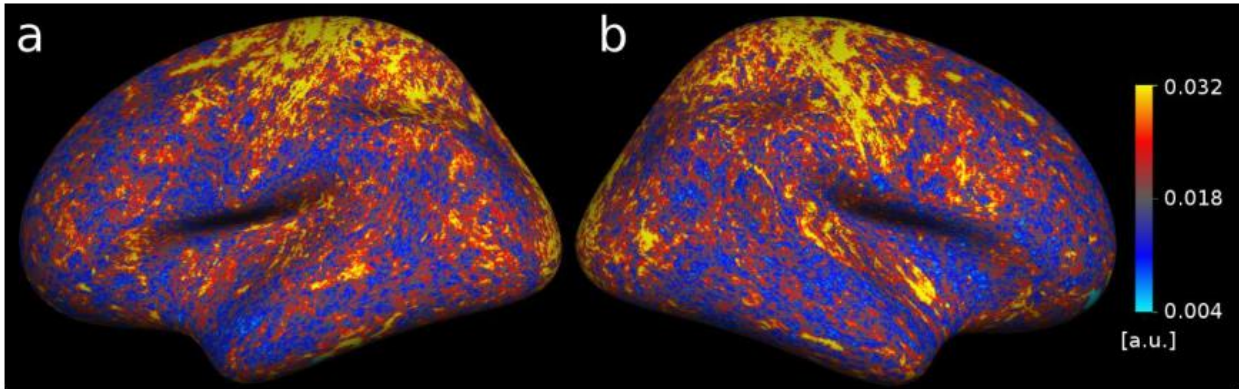
Supporting Figure S2: Group average (N=8) standard deviation of the AFD_{total} maps displayed on an inflated surface, from MSMT-CSD (a: left, b: right hemispheres). A.u.: arbitrary units.